Journal of Non-Newtonian Fluid Mechanics, 29 (1988) 217–244
Elsevier Science Publishers B.V., Amsterdam – Printed in The Netherlands

FINITE ELEMENT EULERIAN–LAGRANGIAN METHOD FOR TIME DEPENDENT FLOW OF MULTIMODE FLUIDS

J.A. SERDAKOWSKI

Division of Engineering, Brown University, Providence, RI 02912 (U.S.A.)
and Chemical Engineering Consultants, E. Greenwich, RI 02818 (U.S.A.)

and

B. CASWELL

Division of Engineering, Brown University, Providence, RI 02912 (U.S.A.)

(Received July 1, 1987; in revised form April 19, 1988)

Summary

This work is directed towards the application of numerical methods to the solution of time-dependent flows of viscoelastic fluids. An Eulerian–Lagrangian method has been developed in which time differences are carried out in the Lagrangian sense on a fixed mass of material occupying the control volume during a single time step. After transformation of the Lagrangian difference equations to the Eulerian description, the spatial dependence of the unknown fields is calculated by the finite element method. The backward Lagrangian time difference automatically builds exact upwinding into the scheme, and reduces the asymmetry of the matrix of coefficients. An important feature of this technique is its applicability to multi-mode fluids whose properties are characterized by a spectrum of relaxation times. In this paper the method is demonstrated with the problem of startup of Poiseuille flow for the Oldroyd-B fluid and for a multimode, rubberlike fluid.

1. Introduction

The Eulerian–Lagrangian scheme given in this paper is a further development of the ideas presented in earlier papers [1,2]. In most flow problems a spatial domain (control volume) defines the system into and out of which material enters and leaves. This situation appears to mandate the Eulerian

0377-0257/88/$03.50

perspective, and the use of a Lagrangian formulation seems counterintuitive. Indeed, a purely Lagrangian numerical formulation inevitably runs into difficulty as time progresses since the original domain becomes highly distorted, as for example in Hassager [3]. In this paper the point of view is Eulerian over a finite time span, but during a short time step the Lagrangian viewpoint is adopted in order to carry out certain critical approximations. To understand this dual perspective it is useful to recall some features of each point of view. At any instant in time the Eulerian observer does not recognize material points; he observes only point values of fields defined over a spatial domain. Simultaneously the Lagrangian observer sees a continuum of material points which exactly coincide with the spatial domain. The conservation laws apply to the material system, and are interpreted in the spatial domain by well-known mathematical transformations. In a continuous formulation a set of particles coincides within the perspective of both the Eulerian and Lagrangian observers at one instant of time. Over a finite interval of time the Eulerian observer will measure, among other things, the effects of a continuous inflow and outflow of material on the fields of the spatial domain. A Lagrangian observer can follow over a finite time Δt a set of particles that coincide with the control volume at time t. Provided the interval Δt is sufficiently small the distortion of this material system can be represented with relatively simple mathematics. The governing Lagrangian equations are solved for their time dependence in a material reference system which is by definition independent of time. The approximate Lagrangian equations are then transformed into their Eulerian equivalents which govern the spatial dependence of the fields defined over the spatial domain. After the Eulerian fields at time t have been obtained the "old" material system is relinquished, and the material which coincides at $t + \Delta t$ with the control volume becomes the "new" system to be followed by the Lagrangian observer over a new time interval Δt. The repetition of this process allows the time evolution of the Eulerian fields to be traced in time by discrete intervals Δt.

In the limit of vanishing Δt the above process reduces to the Eulerian case, and it is necessary to consider what advantages are to be gained from the Lagrangian time step. In the material description convected derivatives are absorbed into total time derivatives, and constitutive equations of the differential type become ordinary differential equations in time. Numerical methods for ordinary differential equations offer a simple approximate solution of the constitutive equation which achieves the uncoupling of the stress variables from velocity and pressure variables. The practical consequence of this feature is that the role of the stresses is reduced to that of auxiliary storage variables, and that the unknowns at any stage are the velocity and pressure, as in the Newtonian problem. This is to be compared

with the mixed method in which stresses, velocity and pressure are simultaneous unknowns in the usual Eulerian finite element formulation. The enormous storage required for the huge matrices generated with the mixed method effectively prohibits the simulation of multimode fluids. The simulation of these fluids presents a difficulty beyond the practical one of storage capacity. Since the spectrum of relaxation times ranges over decades the partial stresses associated with each mode can be characterized approximately in the same flow as being in the slow flow (Rivlin–Ericksen) regime all the way to the fast flow regime (small, fast displacements). It will be shown below that the Eulerian–Lagrangian approximations given in this paper are in fact Padé approximants which contain both the fast and the slow flow limits. Hence a single algorithm can be used over the whole range of time scales in the spectrum. Other important consequences of the Lagrangian time step are the incorporation of the concept of exact upwinding, and the symmetrization of the contributions of the stress terms to the matrix operator of the discrete system.

Examples of the successful application of Lagrangian concepts to other systems can be found in Neuman [4], diffusion–convection equation, and in Huffenus [5], Navier–Stokes equation. In these examples the motivation is to avoid the pitfalls of upwinding in the discretization of the convective terms. Since the diffusional and the viscous terms are retained in their usual spatial forms the convected derivatives are approximated as Lagrangian differences along pathlines with accuracy of $O(\Delta t)$. In [1,2] it is clearly demonstrated that for viscoelastic fluids this level of accuracy is insufficient since the leading terms of the Lagrangian stress approximations are themselves of $O(\Delta t)$. In this work the Lagrangian approximation of the stress for linear viscoelastic fluids will be emphasized; it was shown in [1] how the Lagrangian step can be extended to nonlinear constitutive equations.

2. Eulerian–Lagrangian analysis

Earlier versions of the Eulerian–Lagrangian time marching scheme are described in [1,2], but no numerical examples were presented. The schemes used in this paper will be outlined below, and will be demonstrated with numerical experiments. In each case the schemes have been derived from a Galerkin statement in space and time in order to maintain consistency of the concept and to avoid *ad hoc* developments. This is more important in an Eulerian–Lagrangian formulation than in the purely Eulerian case for which many examples of time marching are to be found in the literature. In these examples time and space are treated separately by differences and by finite elements respectively, and usually the validity of this procedure is unquestioned. In the Eulerian–Lagrangian case space and time are interconnected

other words, spatial operations will not be separate from temporal operations. This is the reason for developing the temporal expansion from the Lagrangian point of view in terms in the Piola stress $\boldsymbol{S}$.

A most convenient material system consists of the material which occupies the spatial control volume at the present time t. This set of particles will be followed over the interval $t-\Delta t/2,\ t+\Delta t/2$. Integration with respect to time in (2.1) can be carried out with the integrand regarded as a function of $\boldsymbol{X}$, and t, the material coordinates $\boldsymbol{X}$ being independent of time. Expansion of the integrand about the present time t gives,

$$\Delta t \int_{V_0} u_i \left\{ S^{Ki}_{,K} - \rho_0 (a^i - b^i) \right\} \mathrm{d}V = \mathrm{O}(\Delta t^3). \tag{2.3}$$

The "0" subscripts signify quantities referred to the $\boldsymbol{X}$ system. The Eulerian form of this momentum statement is easily recovered by means of the chain rule and the following properties of deformation gradients, (Truesdell [16])

$$\left(x^k_{,K}/J\right)_{,k} = 0, \quad \left(X^K_{,k} J\right)_{,K} = 0, \tag{2.4}$$

Integration by parts of the stress term in (2.3) yields the material form of the usual Galerkin equation in which the stresses appear in virtual work terms within the volume and on the surface,

$$\int_{V_0} \left\{ \rho_0 (a^i - b^i) u_i + S^{Ki} u_{i,K} \right\} \mathrm{d}V_0 = \int_{A_0} \mathrm{d}A_K S^{Ki} u_i + \mathrm{O}(\Delta t^2), \tag{2.5}$$

where $\mathrm{d}A_K$ is the vector differential surface element referred to material coordinates. The material form is displayed to emphasize the role of the Piola stress for which approximations will be developed below. The usual Eulerian–Galerkin finite element statement of momentum balance is easily obtained by means of the chain rule and (2.2),

$$\int_V \left[\rho (\boldsymbol{a} - \boldsymbol{b}) \cdot \boldsymbol{u} + \boldsymbol{T} : \nabla \boldsymbol{u} \right] \mathrm{d}V = \int_A \mathrm{d}\boldsymbol{A} \cdot \boldsymbol{T} \cdot \boldsymbol{u} + \mathrm{O}(\Delta t^2). \tag{2.6}$$

When combined with the constraint of incompressibility this equation expresses the conservation laws in terms of Eulerian fields for the material which occupies the control volume at time t.

3. Kinematical preliminaries

Since the only primitive kinematic variable is velocity all other kinematic variables must be constructed from velocity fields. In several situations it will be necessary to extrapolate velocities forward in time from fields stored at previous times. Such extrapolations will be based on Eulerian time expansions of the kind

$$\boldsymbol{V}_* = \boldsymbol{V}' + \Delta t\ \partial \boldsymbol{V}'/\partial t + \left(\Delta t^2/2\right) \partial^2 \boldsymbol{V}'/\partial t^2 + \cdots, \tag{3.1}$$

where Δt is any time increment and the partial time derivatives are approximated by Eulerian differences to the degree of accuracy required,

$$\partial V'/\partial t = (V' - V'')/\Delta t + O(\Delta t) = (3V' - 4V'' + V''')/2\Delta t + O(\Delta t^2), \tag{3.2}$$

$$\partial^2 V'/\partial t^2 = (V' - 2V'' + V''')/\Delta t^2 + O(\Delta t). \tag{3.3}$$

The primes $'$, $''$, $'''$ denote velocities at a spatial point at times $t - \Delta t$, $t - 2\,\Delta t$, $t - 3\,\Delta t$ respectively. Formulae for variable time steps are used, but for simplicity only the case of equal time steps is given here. The subscripts $_*$ will denote velocities extrapolated forward in time, or when iterations are carried out within a time step it will denote the most recently calculated velocity at the current time.

3.1 Displacements

During the course of this work various methods have been tried for the calculation of displacements. The most obvious of these are based on Lagrangian expansions in time for the position of the particle. For example, formula (5.1) of Viriyayuthakorn and Caswell [6] was used in the earlier stages of this work. Such formulae taken over successive discrete intervals of time yield displacements with only Lagrange (C^0) continuity. However, the velocity is a continuous Eulerian field and is simultaneously the Lagrangian time derivative of the displacement. Hence, it should be possible to compute displacements with Hermitian (C^1) continuity. To this end the Hermitian cubic interpolation formula [7] for the relative displacement as a Lagrangian function of time is taken as a starting point,

$$\boldsymbol{U}(\xi) - \boldsymbol{U}_+ = (\boldsymbol{U}_- - \boldsymbol{U}_+)(2 - 3\xi + \xi^3)/4 + \left[(\boldsymbol{V}_+ - \boldsymbol{V}_-)(\xi^2 - 1) + (\boldsymbol{V}_+ + \boldsymbol{V}_-)(\xi^3 - \xi)\right] \Delta t/8, \tag{3.4}$$

where $-1 \leqslant \xi \leqslant 1$, and $\boldsymbol{U}_\pm = \boldsymbol{U}(\pm 1)$ and $\boldsymbol{V}_\pm = \boldsymbol{V}(\pm 1)$ are the positions and velocities of the particle at times t and $t - \Delta t$ respectively. The time derivative of (3.4) yields the temporal interpolation of particle velocity,

$$\boldsymbol{V} = (\boldsymbol{U}_- - \boldsymbol{U}_+)(\xi^2 - 1)3/(2\,\Delta t) + (\boldsymbol{V}_+ - \boldsymbol{V}_-)\xi/2 + (\boldsymbol{V}_+ + \boldsymbol{V}_-)(3\xi^2 - 1)/4. \tag{3.5}$$

At the Gauss points in time along the particle trajectory, $\xi = \pm 1/\sqrt{3}$, evaluation of (3.5) gives

$$\boldsymbol{U}_- - \boldsymbol{U}_+ = -(\boldsymbol{V}_{g+} + \boldsymbol{V}_{g-})\,\Delta t/2 + O(\Delta t^4), \tag{3.6}$$

$$\boldsymbol{V}_+ - \boldsymbol{V}_- = \sqrt{3}\,(\boldsymbol{V}_{g+} - \boldsymbol{V}_{g-}) + O(\Delta t^3). \tag{3.7}$$

Thus the trajectory Gauss point values, $\boldsymbol{V}_{g\pm} = \boldsymbol{V}(\pm 1/\sqrt{3})$, predict the

displacement (3.6) of the particle at $t - \Delta t$ relative to its current position. Equation (3.7) is a consistency relation between the end point velocities and the Gauss point values which guarantees Hermitian continuity at the end points. With the help of (3.6, 7) eqn. (3.4) can be converted into a displacement predictor in terms of velocities,

$$\boldsymbol{U}(\xi) - \boldsymbol{U}_+ = -(\boldsymbol{V}_{g+} + \boldsymbol{V}_{g-})(2 - 3\xi + \xi^3)\,\Delta t/8 + \left[\sqrt{3}(\boldsymbol{V}_{g+} - \boldsymbol{V}_{g-})(\xi^2 - 1) + (\boldsymbol{V}_+ + \boldsymbol{V}_-)(\xi^2 - \xi)\right]\Delta t/8. \tag{3.8}$$

Equations (3.6, 7 and 8) provide the basis for the determination of displacements with Hermitian continuity by means of the following iterative procedure:

i) Assume that values of $\boldsymbol{V}_+$, $\boldsymbol{V}_-$, $\boldsymbol{V}_{g+}$, $\boldsymbol{V}_{g-}$ are in hand, $\boldsymbol{V}_+$, $\boldsymbol{V}_{g+}$, $\boldsymbol{V}_{g-}$ having been extrapolated forward in time by expansions of the type (3.1).

ii) Predict the temporal Gauss point displacements from (3.8).

iii) At the temporal Gauss points interpolate velocity fields at several previous times as required to furnish new values of $\boldsymbol{V}_{g+}$, $\boldsymbol{V}_{g-}$ by means of Eulerian time expansions (3.1).

iv) Predict the endpoint displacement $\boldsymbol{U}_- - \boldsymbol{U}_+$ by means of (3.6), and interpolate the endpoint velocity, $\boldsymbol{V}_-$.

v) Check the consistency condition (3.7) against a predefined tolerance; iterate if required since a new set of velocities is now in hand to begin again at (ii). Clearly, at the start of the process the velocities in (i) are not known. Starting with $\boldsymbol{V}_+$ the Gauss points are estimated to $O(\Delta t)$ and $\boldsymbol{U}_-$ is likewise estimated from (3.6). This is sufficient to begin the iterative process at (i).

3.2 Deformation gradients

The direct method of differentiation of the particle position y at $t - \Delta t$ with respect to its position x as t has been used in this work. This method was used in Viriyayathakorn [6] for very large deformations, and was found to give rise to large errors when accummulated over many time steps. However, in this work it is applied over a single time step only. Other methods have been developed (Malkus [8], Crochet [9], Papanastasiou [10]) which avoid some of the large deformation errors; however, they are restricted to steady flow and have no obvious generalizations to fully three-dimensional deformations. The integration technique of Luo and Tanner [11] is applicable to time-dependent flows, but has not been used in the work reported here.

3.3 Acceleration

In unsteady flow the effects of inertia cannot be discarded even when the Reynolds number of the ultimate steady flow is negligible. Hence it is important to approximate the acceleration with the same attention to accuracy as will be developed for the stress. The Lagrangian time derivative of (3.5) in combination with (3.6) and (3.7) leads to the following formula for the acceleration of a particle at the current instant

$$\boldsymbol{a}(t) = \{(4+\sqrt{3}\,C)\boldsymbol{V} - 3[(1+C)\boldsymbol{V}_{g+} + (1-C)\boldsymbol{V}_{g-}] + (2-\sqrt{3}\,C)\boldsymbol{V}_{-}\}/\Delta t + O(\Delta t^2), \tag{3.9}$$

where C is a constant to be determined. It may be verified that the terms multiplied by C vanish when the Hermitian continuity condition (3.7) is satisfied. The '+' subscript has been omitted in (3.9) from the velocity $\boldsymbol{V}(t)$ to signify its status as an unknown when $\boldsymbol{a}(t)$ is inserted into the momentum statement (2.6). The role of C now becomes clearer since in the acceleration term it determines the degree of implicitness, i.e. the relative weight of the coefficient of the unknown $\boldsymbol{V}$ to the coefficients of the knowns $\boldsymbol{V}_{g+}$, $\boldsymbol{V}_{g-}$ and $\boldsymbol{V}_{-}$. If accuracy is reduced to $O(\Delta t)$ then (3.9) reduces to the simple Lagrangian difference formula,

$$\boldsymbol{a}(t) = (\boldsymbol{V} - \boldsymbol{V}_{-})/\Delta t + O(\Delta t). \tag{3.10}$$

This approximation has been used in Lagrangian formulations [5] of the Newtonian problem for which (3.10) circumvents the well-known difficulties of the numerical treatment of the convective terms which arise from the Eulerian representation of total derivatives. It will be seen below that the accuracy of (3.10) is inadequate for the analysis of viscoelastic flow. For the Newtonian problem it is doubtful that the overhead incurred in the computation of particle displacements required in the Lagrangian formulation compensates for its advantages. For viscoelastic fluids the solution of a nonlinear constitutive equation simultaneously with the conservation laws is greatly simplified by the Lagrangian formulation, and thus compensates for the overhead involved.

4. Stress approximations

Two stress approximations have been tried in this work; they are nominally of $O(\Delta t^2)$ and $O(\Delta t^3)$ respectively. For the lower order case the Piola stress at the current time is approximated by the Lagrangian backward difference

$$\boldsymbol{S}(t) = \boldsymbol{S}_{-} + \Delta t\dot{\boldsymbol{S}}(t) + O(\Delta t^2), \tag{4.1}$$

where $\boldsymbol{S}_- = \boldsymbol{S}(t - \Delta t)$ is the stress for the same particle at the prior time level, and is regarded as known. Since the stresses are stored as Eulerian fields $\boldsymbol{S}_-$ must be constructed from (2.2). The dependence of $\boldsymbol{S}$ on the reference coordinates is suppressed since it is constant during particle motion. The approximations are designed to express the stress increment in terms of known stress and kinematic fields and the unknown velocity field. This is accomplished by use of the constitutive equation to eliminate the stress derivative $\dot{\boldsymbol{S}}(t)$. For many differential models the stress derivative is explicitly given in the material description as,

$$\dot{\Sigma} = \dot{\Sigma}(\Sigma, \dot{\boldsymbol{C}}^{-1}), \quad \Sigma^{KI} = JX^K_{,k} X^I_{,i} T^{ki}, \tag{4.2}$$

where $\boldsymbol{C}^{-1}$ is the Finger strain relative to the current configuration. For other models the elimination of the stress derivative is less obvious, and it may be necessary to define other auxiliary stress variables in order to proceed. For example, for the linear visco-elastic fluid with a spectrum of relaxation times it is necessary to define one stress field for each relaxation mode [1]. In this paper the approximation will be developed only for the Maxwell fluid for which the Piola stress is given by

$$\lambda \dot{\boldsymbol{S}} = \eta \dot{\boldsymbol{B}}^{-1} - \boldsymbol{S} + \lambda \boldsymbol{S} \cdot \boldsymbol{L}^{\mathrm{T}}, \tag{4.3}$$

where $\boldsymbol{L}$ is the spatial velocity gradient $\partial \boldsymbol{V}/\partial \boldsymbol{x}$, and $\dot{\boldsymbol{B}}$ is related to $\dot{\boldsymbol{C}}^{-1}$ by

$$\dot{B}^{Ki} = -\dot{C}^{-1KI} x^i_{,I}. \tag{4.4}$$

Elimination of $\dot{\boldsymbol{S}}$ in the expansion (4.1) with the constitutive equation (4.3) leads to

$$D(\Delta t/\lambda)\boldsymbol{S} \cdot (\boldsymbol{I} - \Delta t \boldsymbol{L}^{\mathrm{T}}) = \boldsymbol{S}_- + \dot{B}\eta \, \Delta t/\lambda + \mathrm{O}(\Delta t^2), \tag{4.5}$$

$$D(u) = 1 + u + \mathrm{O}(u^2). \tag{4.6}$$

The retention of the factor $D(\Delta t/\lambda)$ rather than unity will be elucidated below. It follows from (4.5) that the Piola stress at the current time is given explicitly as

$$\boldsymbol{S} = \left\{ \boldsymbol{S}_- \cdot \frac{\partial \boldsymbol{x}^{\mathrm{T}}}{\partial \boldsymbol{y}} + \Delta t \boldsymbol{S} \cdot \frac{\partial \boldsymbol{x}^{\mathrm{T}}}{\partial \boldsymbol{y}} \cdot (\boldsymbol{L}^{\mathrm{T}} - \boldsymbol{L}^{\mathrm{T}}_*) + \dot{\boldsymbol{B}}\eta \, \Delta t/\lambda \right\} / D(\Delta t/\lambda) + \mathrm{O}(\Delta t^2), \tag{4.7}$$

where the deformation gradient $\partial \boldsymbol{x}/\partial \boldsymbol{y} = \boldsymbol{I} + \Delta t \boldsymbol{L}_* + \mathrm{O}(\Delta t^2)$, and the asterisk subscripts imply that the velocity gradient $\boldsymbol{L} = \partial \boldsymbol{V}/\partial \boldsymbol{x}$ is evaluated with the known velocity $\boldsymbol{V}_*(\boldsymbol{x}, t)$ defined in (3.1). By inversion of (2.2) the true stress for the particle at times t and $t - \Delta t$ is given respectively by

$$\boldsymbol{T}(\boldsymbol{x}, t) = \frac{\partial \boldsymbol{x}}{\partial \boldsymbol{X}} \cdot \boldsymbol{S}(\boldsymbol{X}, t)/J, \quad \boldsymbol{T}(\boldsymbol{y}, t) = \frac{\partial \boldsymbol{y}}{\partial \boldsymbol{X}} \cdot \boldsymbol{S}(\boldsymbol{X}, t - \Delta t)/J_-, \tag{4.8}$$

$$J_- = \det \left| y^k_{,K} \right|. \tag{4.9}$$

From (4.8) it follows that (4.7) can be transformed into the Eulerian form,

$$\boldsymbol{T} = \left(\frac{\partial \boldsymbol{x}}{\partial \boldsymbol{y}} \cdot \boldsymbol{T}_{-} \cdot \frac{\partial \boldsymbol{x}^{\mathrm{T}}}{\partial \boldsymbol{y}} \cdot \left[\boldsymbol{I} + (\boldsymbol{L}^{\mathrm{T}} - \boldsymbol{L}_{*}^{\mathrm{T}})\, \Delta t \right] + \boldsymbol{A}\eta\, \Delta t/\lambda \right) / D(\Delta t/\lambda) + \mathrm{O}(\Delta t^2). \tag{4.10}$$

In this result the incompressibility constraint has been anticipated by the setting to unity of the volume ratio in the transformations (4.8). Inspection of (4.10) shows that it is a useful and suitably linearized formula for the stress. In a time stepping scheme $\boldsymbol{T}_{-}$, $\boldsymbol{L}_{*}$, $\partial \boldsymbol{x}/\partial \boldsymbol{y}$ are determined from stored stress and velocity fields at previous time levels, the unknown velocity $\boldsymbol{V}(\boldsymbol{x}, t)$ appears in $\boldsymbol{L}$ and the strain rate $\boldsymbol{A}$. Once $\boldsymbol{V}(\boldsymbol{x}, t)$ has been calculated (3.10) can be used to construct the stress at time t, and thereby set the stage for the next time step. Although the development given above is directed toward the solution of the spatial field equations by the finite element method, eqn. (4.10) can equally be the basis for treating the spatial problem by finite differences. In the finite element method (4.10) is substituted into the virtual work term of (2.6), and the unknown velocity field can be shown to satisfy the self-adjointness property which ensures only symmetric contributions to the matrix operator. It will be seen below that the same terms generate non-symmetric matrix contributions on certain boundaries. This symmetrization of terms which are strongly convective is one of the most remarkable aspects of the Eulerian–Lagrangian formulation, and is also found in Neuman's [4] formulation of the convection–diffusion equation. The corresponding stress approximation for the Oldroyd-B fluid is easily obtained since it is the weighted sum of the Maxwell stress and the Newtonian stress,

$$\boldsymbol{T} = (1 - a)\boldsymbol{T}_{\mathrm{M}} + a\eta \boldsymbol{A}. \tag{4.11}$$

The parameter $0 \leqslant a \leqslant 1$ is the retardation/relaxation ratio and $\boldsymbol{T}_{\mathrm{M}}$ is the Maxwell stress with viscosity η and relaxation time λ. In the case of the multimode linear viscoelastic fluid (Lodge [12] rubberlike fluid) with relaxation spectrum $(\lambda_i, \eta_i;\ i = 1, N)$ the partial stress $\boldsymbol{T}_i$ for each mode is a Maxwell stress, and hence will be given by (4.10) with the appropriate parameters λ_i, η_i. It follows that for a multimode fluid, storage space must be provided for N partial stresses. However, since the stresses are not unknowns in the solution of the spatial field equations the size of the matrix of coefficients will be determined only by the size of the vector of unknown velocities and pressures regardless of the number of modes in the relaxation spectrum.

Numerical experiments based on (4.10) were carried out early in the development of the Eulerian–Lagrangian method. Errors for problems hav-

ing analytical solutions were studied as functions of Δt, it was found that the convergence rate was $O(\Delta t)$ rather than $O(\Delta t^2)$ as indicated in (4.10). While the quality of the numerical solutions is affected by several factors which will be discussed later, at least one type of error can be understood on the basis of the time development alone. To understand this it is sufficient to consider the following one-dimensional flow of a "fluid" which differs from the Maxwell fluid by a single term

$$T + \lambda T_t - \epsilon \lambda^2 T_{tt} = \eta W_r, \quad T = T(r, t), \quad W = W(r, t), \tag{4.12}$$

where T is the shear stress, W the velocity, r the coordinate across the pathlines, and the subscripts stand for the partial derivatives with respect to r, t. To obtain a stress approximation for the fluid defined by this equation the starting point is again (4.1), but because of the second time derivative in (4.12) the term in Δt^2 is retained. It can be shown that, if $\epsilon = \Delta t/2\lambda$, the stress approximation for this fluid is identical to (4.10). In other words, the approximation (4.10) is the same for two fluids which differ by a term $O(\Delta t)$. The character of this error is not easily classified; at long times it contributes a diffusive effect to the solution of the one-dimensional problem. In order to control this hidden error (4.1) is replaced by the more accurate formula for the stress at time t

$$\boldsymbol{S} = \boldsymbol{S}_- + \left(\dot{\boldsymbol{S}} + \dot{\boldsymbol{S}}_-\right) \Delta t/2 + O(\Delta t^3). \tag{4.13}$$

The Maxwell constitutive equation (4.3) evaluated for the same particle at $t - \Delta t$ can be written with accuracy sufficient for use in (4.13) as

$$\lambda \dot{\boldsymbol{S}}_- = \eta \dot{\boldsymbol{B}}_-^{-1} - \boldsymbol{S} + \Delta t \dot{\boldsymbol{S}} + \lambda \boldsymbol{S}_- \cdot \boldsymbol{L}_-^{\mathrm{T}} + O(\Delta t^2). \tag{4.14}$$

The approximation here is the replacement of $\boldsymbol{S}_-$ with $\boldsymbol{S} - \Delta t \dot{\boldsymbol{S}} + O(\Delta t^2)$ to achieve a more strongly implicit result in the final formula. The velocity gradient $\partial V_-/\partial y$ at $(y, t - \Delta t)$ is denoted by $\boldsymbol{L}_-$. Elimination of $\dot{\boldsymbol{S}}$ and $\dot{\boldsymbol{S}}_-$ in (4.13) by means of (4.3) and (4.14) respectively yields

$$\begin{aligned} D(\Delta t/\lambda)\boldsymbol{S} \cdot \left(\boldsymbol{I} - \boldsymbol{L}^{\mathrm{T}} \Delta t/2\right) &= \boldsymbol{S}_- \cdot \left(\boldsymbol{I} + \boldsymbol{L}_-^{\mathrm{T}} \Delta t/2\right) \\ &+ \left[\dot{\boldsymbol{B}}_- + (1 + \Delta t/\lambda)\dot{\boldsymbol{B}}\right] \Delta t \eta/2\lambda + O(\Delta t^3), \end{aligned} \tag{4.15}$$

where $$D(u) = 1 + u + 1/2\ u^2 = e^u + O(u^3). \tag{4.16}$$

Postmultiplication by $(\boldsymbol{I} - \boldsymbol{L}^{\mathrm{T}} \Delta/2)^{-1}$ and retention only of terms correct to $O(\Delta t^3)$ provides the desired explicit formula for the Piola stress at the current time,

$$\begin{aligned} D(\Delta t/\lambda)\boldsymbol{S} = \boldsymbol{S}_- &\cdot \left(\boldsymbol{I} + \boldsymbol{L}^{\mathrm{T}} \Delta t/2\right) \cdot \left(\boldsymbol{I} - \boldsymbol{L}^{\mathrm{T}} \Delta t/2\right)^{-1} \\ &+ \left(\dot{\boldsymbol{B}}_- + \dot{\boldsymbol{B}}\right) \cdot \left(\boldsymbol{I} + \boldsymbol{L}^{\mathrm{T}} \Delta t/2\right) \eta\ \Delta t/2\lambda \\ &+ \dot{\boldsymbol{B}} (\Delta t/\lambda)^2 \eta/2 + O(\Delta t^3). \end{aligned} \tag{4.17}$$

Transformation of (4.17) into a form, analogous to (4.10), which expresses the true stress as a function of Eulerian fields begins with eqns. (B.6, B.7). Appendix B of [1] by which the deformation gradient relating points $\boldsymbol{y} = \boldsymbol{r}(\boldsymbol{X}, t - \Delta t)$ and $\boldsymbol{x} = \boldsymbol{r}(\boldsymbol{X}, t)$ is obtained as the central product formula,

$$\boldsymbol{F} = (\boldsymbol{I} - \boldsymbol{L}\,\Delta t/2)^{-1} \cdot (\boldsymbol{I} + \boldsymbol{L}_{-}\,\Delta t/2) + \mathrm{O}(\Delta t^3). \tag{4.18}$$

This is the transpose of the postmultiplier of the first term on the right hand side of (4.17). Since (4.18) is nonlinear with respect to the unknown velocity $\boldsymbol{V}(\boldsymbol{x}, t)$ it is linearized in the sense of spatial Newtonian iterations as follows

$$\boldsymbol{F}^{\mathrm{T}} = \frac{\partial \boldsymbol{x}^{\mathrm{T}}}{\partial \boldsymbol{y}} + \frac{\partial \boldsymbol{x}^{\mathrm{T}}}{\partial \boldsymbol{y}} \cdot (\boldsymbol{L}^{\mathrm{T}} - \boldsymbol{L}^{\mathrm{T}}_{*})\,\Delta t/2 + \mathrm{O}(\Delta t^3), \tag{4.19}$$

where it is assumed that the difference $\boldsymbol{L}^{\mathrm{T}} - \boldsymbol{L}^{\mathrm{T}}_{*}$ is at most $\mathrm{O}(\Delta t)$. As in (4.10) the notation $\partial \boldsymbol{x}/\partial \boldsymbol{y}$ for the deformation gradients implies that $\boldsymbol{y}$ has been determined from known velocity fields.

The second term in (4.17) is likewise linearized with respect to the unknown velocity $\boldsymbol{V}(\boldsymbol{x}, t)$ as

$$\begin{aligned}(\dot{\boldsymbol{B}}_{-} + \dot{\boldsymbol{B}}) \cdot (\boldsymbol{I} + \boldsymbol{L}^{\mathrm{T}}\,\Delta t/2) = 2\dot{\boldsymbol{B}}_0 \cdot \frac{\partial \boldsymbol{x}^{\mathrm{T}}}{\partial \boldsymbol{z}} \cdot \left[\boldsymbol{I} + (\boldsymbol{L}^{\mathrm{T}} - \boldsymbol{L}^{\mathrm{T}}_{*})\,\Delta t/2\right] \\ + \dot{\boldsymbol{B}} - \dot{\boldsymbol{B}}_{*} + \mathrm{O}(\Delta t^2)\end{aligned} \tag{4.20}$$

consistent with (4.19), $\dot{\boldsymbol{B}} - \dot{\boldsymbol{B}}_{*}$ is assumed to be at most $\mathrm{O}(\Delta t)$, and

$$2\dot{\boldsymbol{B}}_0 = \dot{\boldsymbol{B}}_{-} + \dot{\boldsymbol{B}}_{*}; \quad \frac{\partial \boldsymbol{x}}{\partial \boldsymbol{z}} = \boldsymbol{I} + \boldsymbol{L}_{*}\,\Delta t/2 + \mathrm{O}(\Delta t^2). \tag{4.21}$$

The strain rate $\dot{\boldsymbol{B}}_0$ and the deformation gradient $\partial \boldsymbol{x}/\partial \boldsymbol{z}$ refer to the midpoint in time $t - \Delta t/2$ with position $\boldsymbol{z} = \boldsymbol{r}(\boldsymbol{X}, t - \Delta t/2)$ along the particle trajectory, and are estimated by (4.21) with sufficient accuracy for use in (4.17). When (4.8) and (4.19–21) are used in (4.17) together with

$$2\,\frac{\partial \boldsymbol{x}}{\partial \boldsymbol{X}} \cdot \boldsymbol{B}_0 \cdot \frac{\partial \boldsymbol{x}^{\mathrm{T}}}{\partial \boldsymbol{z}} = 2\frac{\partial \boldsymbol{x}}{\partial \boldsymbol{z}} \cdot \boldsymbol{A}_0 \cdot \frac{\partial \boldsymbol{x}^{\mathrm{T}}}{\partial \boldsymbol{z}} = \frac{\partial \boldsymbol{x}}{\partial \boldsymbol{y}} \cdot \boldsymbol{A}_{-} \cdot \frac{\partial \boldsymbol{x}^{\mathrm{T}}}{\partial \boldsymbol{y}} + \boldsymbol{A}_{*} + \mathrm{O}(\Delta t^2), \tag{4.22}$$

there results the following approximation for the true stress,

$$\begin{aligned}\boldsymbol{T} = \Bigg\{ &\frac{\partial \boldsymbol{x}}{\partial \boldsymbol{y}} \cdot \boldsymbol{H}_{-} \cdot \frac{\partial \boldsymbol{x}^{\mathrm{T}}}{\partial \boldsymbol{y}} \cdot \left[\boldsymbol{I} + (\boldsymbol{L}^{\mathrm{T}} - \boldsymbol{L}^{\mathrm{T}}_{*})\,\Delta t/2\right] \\ &+ \boldsymbol{A}_{*} \cdot \left[(\boldsymbol{L}^{\mathrm{T}} - \boldsymbol{L}^{\mathrm{T}}_{*})\,\Delta t/2\right] \eta\,\Delta t/2\lambda \\ &+ \boldsymbol{A}(1 + \Delta t/\lambda)\eta\,\Delta t/2\lambda \Bigg\} / D(\Delta t/\lambda) + \mathrm{O}(\Delta t^3)\end{aligned} \tag{4.23}$$

in which $\boldsymbol{H}_{-}$ is the value at $\boldsymbol{y}$, $t - \Delta t$ of

$$\boldsymbol{H} = \boldsymbol{T} + \boldsymbol{A}\eta\,\Delta t/2\lambda. \tag{4.24}$$

Although the error in (4.23) is nominally $O(\Delta t^3)$ it is clear that an error of $O(\Delta t^2)$ can be inferred by an argument similar to that given above to demonstrate the error $O(\Delta t)$ hidden in (4.10). While the above derivation contains certain steps such as (4.14) which appear to be arbitrary the same result has been derived by a completely different approach not given here. A unique feature of both (4.10) and (4.23) is that the exact stress system for steady shearing flow is recovered in the limit $\Delta t/\lambda \to \infty$. The factor $D(\Delta t/\lambda)$ in (4.6) and (4.16) plays the key role in ensuring this property which gives (4.10) and (4.23) the character of Padé approximants rather than algebraic approximations in powers of Δt. In the case of multimode fluids this property is essential since the λ_i of the spectrum typically span many decades. If Δt is selected to be a small fraction of the mean relaxation time then $\Delta t/\lambda_i$ will be very large for the modes of the spectrum with $\lambda_i \ll \Delta t$.

5. Incompressibility constraint

The stress for the general linear viscoelastic fluid is written in terms of the Finger strain relative to the current configuration,

$$\boldsymbol{T} = -G_0\boldsymbol{I} + \int_{-\infty}^{t} \mu(t-t')\boldsymbol{C}^{-1}(t, t')\,\mathrm{d}t', \tag{5.1}$$

where $\mu(s) = -\mathrm{d}G(s)/\mathrm{d}s$, $G_0 = G(0)$ and $G(s)$ is the relaxation function. The dependence of $\boldsymbol{C}^{-1}$ on position is suppressed in these equations. For incompressible flow the stress is arbitrary to within a scalar isotropic pressure. In axisymmetric flow $C_{\theta\theta}^{-1}$ is a principal value of the strain, and hence a scalar invariant. In a Galerkin formulation the volume ratio J is formally treated as a variable, and hence a valid scalar pressure for axisymmetric flow is then

$$P = \int_{-\infty}^{t} \mu(t-t')C_{\theta\theta}^{-1}(t, t')J(t, t')\,\mathrm{d}t'. \tag{5.2}$$

Upon addition of (5.2) to the isotropic part of (5.1) there results a Galerkin modification of (5.1) for axisymmetric motions,

$$\boldsymbol{T} = -\left\{G_0 + \int_{-\infty}^{t} \mu(t-t')C_{\theta\theta}^{-1}(t, t')[J(t, t') - 1]\,\mathrm{d}t'\right\}\boldsymbol{I} + \int_{-\infty}^{t} \mu(t-t')\boldsymbol{C}_2^{-1}(t, t')\,\mathrm{d}t', \tag{5.3}$$

where $\boldsymbol{C}_2^{-1}(t, t')$ lies entirely in the r–z plane and has components

$$\boldsymbol{C}_2^{-1} = \begin{pmatrix} C_{rr}^{-1} - C_{\theta\theta}^{-1} & 0 & C_{rz}^{-1} \\ \cdot & 0 & 0 \\ \cdot & \cdot & C_{zz}^{-1} - C_{\theta\theta}^{-1} \end{pmatrix} \tag{5.4}$$

The strain form (5.3) can be put into the strain rate form by means of an integration by parts,

$$\boldsymbol{T} = -\boldsymbol{I}(P + G_0) + \boldsymbol{T}_2, \tag{5.5}$$

$$\boldsymbol{T}_2 = \int_{-\infty}^{t} G(t-t')\dot{\boldsymbol{C}}_2^{-1}(t, t')\,\mathrm{d}t',$$

$$P = \int_{-\infty}^{t} G(t-t')\,\overline{C_{\theta\theta}^{-1}(t, t')[1 - J(t, t')]}\,\mathrm{d}t' \tag{5.6}$$

It follows from (5.4) that $\boldsymbol{T}_2$ is also an in plane tensor, and that the isotropic part of (5.5) is the only three-dimensional to $\boldsymbol{T}$. For the Maxwell fluid the integrals (5.6) can be expressed as the differential equations,

$$\boldsymbol{T}_2 + \lambda \overset{\nabla}{\boldsymbol{T}}_2 = \eta \boldsymbol{A}_2, \quad P + \lambda \dot{P} = -\eta \nabla \cdot \boldsymbol{v}, \tag{5.7}$$

where $\boldsymbol{A}_2$ is obtained by material differentiation of (5.4) with respect to time,

$$\boldsymbol{A}_2 = \begin{pmatrix} 2(\partial U/\partial r - U/r) & \partial U/\partial z + \partial W/\partial r \\ & 2(\partial W/\partial z - U/r) \end{pmatrix}. \tag{5.8}$$

Here, U, W are the components of velocity referred to axisymmetric coordinates r, z, and the rate ∇ denotes the upper convective Oldroyd derivative. In axisymmetric flow the approximations (4.10) and (4.23) developed above are applied to the in-plane stress $\boldsymbol{T}_2$ rather than the whole stress tensor. A parallel development of (5.7b) for the Galerkin scalar pressure P reads

$$P(\boldsymbol{x}, t) = \{P_- - \nabla_- \cdot \boldsymbol{v}_- \eta\, \Delta t/2\lambda - \nabla \cdot \boldsymbol{v}(1 + \Delta t/\lambda)\eta\, \Delta t/2\lambda\}/D(\Delta t/\lambda), \tag{5.9}$$

where P_- denotes $P(\boldsymbol{y}, t - \Delta t)$ and ∇_- denotes $\partial/\partial \boldsymbol{y}$. In addition to the Galerkin pressure (5.9) derived from the constitutive equation an incompressible fluid admits a further pressure determined by the boundary conditions. Hence total stress for axisymmetric flow is written as

$$-\{p - [\nabla \cdot \boldsymbol{v}(1 + \Delta t/\lambda)\eta\, \Delta t/2\lambda]/D(\Delta t/\lambda)\}\boldsymbol{I} + \boldsymbol{T}_2. \tag{5.10}$$

This form for the stress is obtained by addition of the in-plane stress to an isotropic stress consisting of (5.9) and an unknown scalar. Since P_- and $\nabla_- \cdot v_-$ are known the first two terms in (5.9) have been absorbed into the unknown pressure p.

The incompressibility constraint is slightly altered from its usual form since $-p$ is effectively the $\theta\theta$-component of total stress. The constraint used in this work is

$$0 = \nabla \cdot \boldsymbol{v}\{h + (2u/r - \nabla \cdot \boldsymbol{u})[(1 + \Delta t/\lambda)\eta\, \Delta t/2\lambda]/D(\Delta t/\lambda)\}, \tag{5.11}$$

where h is the trial function for pressure, and $\boldsymbol{u}$ is the trial function for velocity with components u, w. Both u/r and $\nabla \cdot \boldsymbol{u}$ are scalar invariants of $\nabla \boldsymbol{u}$ in axisymmetric flow. It should be realized that the Galerkin scalar pressure defined in (5.6) and approximated in (5.9), and the constraint (5.11) represent one of many possible ways of imposing incompressibility on the velocity field. The formulation used in this work is motivated by the desire to have the diagonal terms of $\boldsymbol{T}_2$ be stress differences relative to $T_{\theta\theta}$, and the need to maintain the self-adjointness of the pressure terms.

In the Galerkin statement of the momentum equation (2.6) the stress contributes to the virtual work terms within the volume and on the boundary. The latter will be dealt with later. For axisymmetric flows, of this work, $\boldsymbol{x} = \{r, \theta, z\}$, $\boldsymbol{y} = \{R, \Theta, Z\}$; the combination of the volumetric constraint (5.11) and the total stress (5.10) with the in-plane stress approximated by (4.23) yields for the volume virtual work

$$
\begin{aligned}
&-\left(p - \frac{(1+\Delta t/\lambda)\eta\ \Delta t/2\lambda}{D}\nabla \cdot \boldsymbol{v}\right)\nabla \cdot \boldsymbol{u} \\
&-\left(h + \frac{(1+\Delta t)\eta\ \Delta t/2\lambda}{D}(2u/r - \nabla \cdot \boldsymbol{u})\right)\nabla \cdot \boldsymbol{v} + \boldsymbol{T}_2 : \nabla \boldsymbol{u} \\
&= \frac{1}{D}\left\{\left(\frac{\partial \boldsymbol{x}}{\partial \boldsymbol{y}} \cdot \boldsymbol{H}_- \cdot \frac{\partial \boldsymbol{x}^{\mathrm{T}}}{\partial \boldsymbol{y}}\right) : \nabla \boldsymbol{u} + \left(\frac{\partial \boldsymbol{x}}{\partial \boldsymbol{y}} \cdot \boldsymbol{H}_- \cdot \frac{\partial \boldsymbol{x}^{\mathrm{T}}}{\partial \boldsymbol{y}}\right.\right. \\
&\quad \left. + \boldsymbol{A}_{2*}\eta\ \Delta t/2\lambda\right) : \left[(\boldsymbol{L}^{\mathrm{T}} - \boldsymbol{L}_*^{\mathrm{T}}) \cdot \nabla \boldsymbol{u}\right] \\
&\quad \left. + (1 + \Delta t/\lambda)\eta\ \Delta t/2\lambda\left(\boldsymbol{A}_{\mathrm{p}} : \nabla \boldsymbol{u} + 2\Delta \cdot \boldsymbol{v}\,\Delta \cdot \boldsymbol{u}\right)\right\} - p\nabla \cdot \boldsymbol{u} - h\nabla \cdot \boldsymbol{v}, \\
&D = D(\Delta t/\lambda),
\end{aligned}
\tag{5.12}
$$

where $\boldsymbol{A}_{\mathrm{p}}$ is the in-plane strain rate

$$
\boldsymbol{A}_{\mathrm{p}} = \begin{pmatrix} 2\partial U/\partial r & \partial U/\partial z + \partial W/\partial r \\ \cdot & 2\partial W/\partial \zeta \end{pmatrix}, \quad 2\Delta \cdot \boldsymbol{v} = \mathrm{tr}(\boldsymbol{A}_{\mathrm{p}}), \quad \Delta \cdot \boldsymbol{u} = \frac{\partial u}{\partial r} + \frac{\partial w}{\partial z} \tag{5.13}
$$

and the components of $\boldsymbol{H}_-$ are evaluated at $\boldsymbol{y}$, $t - \Delta t$ from

$$
\boldsymbol{H} = \begin{pmatrix} T_{2rr} + A_{2rr}\eta\ \Delta t/2\lambda & T_{rz} + A_{rz}\eta\ \Delta t/2\lambda \\ \cdot & T_{2zz} + A_{2zz}\eta\ \Delta t/2\lambda \end{pmatrix}. \tag{5.14}
$$

The stress and strain rate differences are defined by

$$
\begin{aligned}
&T_{2rr} = T_{rr} - T_{\theta\theta}, \quad T_{2zz} = T_{zz} - T_{\theta\theta} \\
&A_{2rr} = 2\partial U/\partial r - 2U/r, \quad A_{2zz} = 2\partial W/\partial z - 2U/r,
\end{aligned}
\tag{5.15}
$$

and the deformation gradient $\partial x/\partial y$ is obtained by inversion of

$$\frac{\partial y}{\partial x} = \begin{pmatrix} \partial R/\partial r & \partial R/\partial z \\ \partial Z/\partial r & \partial Z/\partial z \end{pmatrix}. \tag{5.16}$$

The virtual work as expressed in (5.12) consists of three contributions. The first term is essentially the work done on the particle by the stresses up to time $t - \Delta t$. The second term accounts for the change in the deformation gradient relative to its estimate at the current time. It is the work due to the instantaneous change of the current configuration. The third term represents the work done by the increment of elastic stress. The coefficient $\eta(D-1)$ approaches $(\eta/\lambda)\,\Delta t$ as $\Delta t \to 0$; if Δt is carried through the gradient operator then $\Delta t \boldsymbol{A}_p$ becomes the analogous operator on the displacements. Hence the term becomes identical to linear elasticity. The last terms are the pressure and volume constraint terms in their usual form. When the unknowns v, p are interchanged with their respective trial functions u, h the virtual work (5.12) is unchanged. Hence in the finite element formulation virtual work contributes only symmetric terms to the matrix of coefficients.

6. Initial conditions and boundary conditions

The initial condition envisioned is the rest state with null stresses. The flow problems to be studied are initial value problems starting from rest and driven by overall pressure differences prescribed as functions of time. In order to be able to impose these conditions on interior flows it is necessary to consider situations in which inlets and outlets are configured to be regions of pure shearing flow or uniform rigid motion. Since the streamwise velocity is not specified on the inlet and outlet sections the prescribed pressure is imposed through the surface integral of the Galerkin statement (2.6). It is assumed that at the inlet/outlet sections the particle pathlines are normal to the cross-stream cut, and velocities have zero spatial derivatives in the pathline direction, consistent with the assumption of pure shearing flow.

Here the development will be carried out for the case in which the inlet/outlet pathlines coincide with the z-direction of an axisymmetric flow. After imposing the pure shearing requirement of zero for U and u, the cross-stream velocity and the trial function respectively, the integrand of the surface virtual work term in (2.6) becomes,

$$\begin{aligned}(p - T_{2zz})w = \Bigg\{ -p + \frac{1}{D(\Delta t/\lambda)} \Bigg[T^-_{2zz} - 2\frac{\partial Z}{\partial r}\left(T^-_{rz} + \eta\, \Delta t/2\lambda \frac{\partial W_-}{\partial r} \right) \\ + \Delta t/2 \left(T^-_{rz} + \eta\, \Delta t/2\lambda \left(\frac{\partial W_-}{\partial r} + \frac{\partial W_*}{\partial r} \right) \right) \Bigg] \left(\frac{\partial W}{\partial r} - \frac{\partial W_*}{\partial r} \right) \Bigg\} w.\end{aligned} \tag{6.1}$$

Consistent with previous notation W, W_* and W_- are axial velocities; the unknown at t, the value at t extrapolated according to (3.1), and the value at $t-\Delta t$ respectively. In a pure shear flow the particle velocity at y, $t-\Delta t$ is identical to its value at x, $t-\Delta t$ since W is unchanged along any pathline. In (5.16) the pressure p is prescribed and T^-_{2zz}, T^-_{rz}, W_*, W_- are known and thus all terms will contribute to the load vector except those containing the unknown W which will contribute to the matrix operator. Velocity boundary conditions are applied in the standard way.

7. Finite element implementation

The algorithms developed above can be implemented by adapting any available finite element code designed to compute steady flows of Newtonian fluids. The essential new features which must be added are:

i. the logic required to track particles and construct the distorted states of elements.

ii. provision for the storage of several velocity and stress fields.

In this work triangular elements are used in the Wilson arrangement of four to a quadrilateral as described in Nickel [13]. Within the triangles velocities and extra stresses are interpolated as quadratic functions of the space variables, and the scalar pressure is interpolated linearly. At element boundaries the velocities and pressures are C_0 continuous functions whereas the stresses are C_{-1} discontinuous functions.

The algorithms for the stress summarized in (4.10), or (4.23) combined with (4.11), the momentum statement (2.6) and the volumetric constraint (5.11) lead to a global system of algebraic equations of the form

$$f\left(\boldsymbol{V},\ \boldsymbol{p},\ \boldsymbol{V}_*,\ \boldsymbol{V}_-,\ \frac{\partial \boldsymbol{x}}{\partial \boldsymbol{y}}\boldsymbol{T}_-\frac{\partial \boldsymbol{x}^{\mathrm{T}}}{\partial \boldsymbol{y}}\right)=0, \tag{7.1}$$

where $\boldsymbol{V}$, $\boldsymbol{p}$ are the vectors of unknown nodal velocities and pressures, and $\boldsymbol{V}_*$, $\boldsymbol{V}_-$, $\partial \boldsymbol{x}/\partial \boldsymbol{y}$, $\boldsymbol{T}_-$ are integration point values of quantities derivable from previously computed nodal values of velocity and stress. The velocity $\boldsymbol{V}_*$ is the extrapolated value of $\boldsymbol{V}$, and is obtained from (3.1–3) in the form,

$$\boldsymbol{V}_* = \boldsymbol{V}_*(\boldsymbol{V}',\ \boldsymbol{V}'',\ \boldsymbol{V}'''). \tag{7.2}$$

Here $\boldsymbol{V}'$, $\boldsymbol{V}''$, $\boldsymbol{V}'''$ are the stored nodal velocity vectors at three previous time levels. For every element the nodal positions R, Z at $t-\Delta t$ are found from the algorithm based on (3.6, 7) described above; the distortion of typical elements is depicted in Fig. 1. Note that by computing the nodal displacements the mesh at $t-\Delta t$ is constructed to have the same edge compatibility as the original mesh. Once the nodal displacements are computed the velocity and stress at $t-\Delta t$, $\boldsymbol{V}_-$ and $\boldsymbol{T}_-$ are interpolated from the

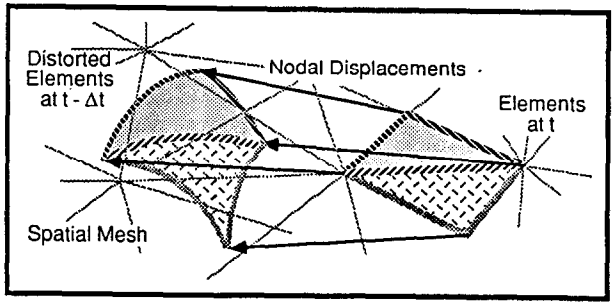

Fig. 1. Typical material element distortion at time $t - \Delta t$, relative to t.

fields in storage. Even though the stresses are stored as discontinuous functions their interpolation along the edges of the distorted elements creates an effectively continuous stress field at $t - \Delta t$. The deformation gradient $\partial x/\partial y$ is computed by inversion of (5.16); the differentiations are carried out with R, Z taken as quadratic functions of r, z.

Since (4.10) or (4.23) and the acceleration (3.9) are linear in V the global system (7.1) is likewise linear in V, p, and after appropriate application of boundary conditions can be solved by standard methods for the field $V(x, t)$. The creation of a linear system (7.1) has been accomplished, with the exception of (4.19), by means of Lagrangian expansions in time. It should not be concluded that the effect of convective nonlinearities, which so dominate the Eulerian formulation, have vanished completely. This is verifiable by iteration on (7.1) with V_* replaced by the most recently determined $V(x, t)$. In the case of linear viscoelasticity experience indicates two iterations per time step to be sufficient. When the constitutive equation (4.2) is nonlinear these iterations within a time step are used to solve the approximation equivalent to (4.10) or (4.23) which are then non-linear. This is dealt with in [1].

Once $V(x, t)$ has become stationary the next task is the updating of the stress field. In (4.10) and (4.23) V_* is taken as equal to V, and they become explicit formulae for the stress $T(x, t)$ in terms of known quantities. Following the same procedure used to set up the system (7.1) the stresses are computed in each element at the seven integration points used in the spatial integration. Since the stress interpolation is discontinuous at element boundaries the nodal stresses can be determined element-by-element. In the work of this paper the six nodal values are obtained by a least squares fit of the seven spatial Gauss point values. In an earlier formulation the stresses were interpolated as linear, discontinuous functions, fitted by least squares to values calculated at the six points of the formula which had been employed for spatial integration. Experiments with linear interpolation of

the stress gave fairly good results in the flow problem described below. However, convergence was limited to relatively low values of the relaxation time. From the few analytical solutions available for viscoelastic fluids it is clear that stress fields will generally require higher order interpolation compared to the corresponding Newtonian problem. The updating of the stress completes the time step, and sets the stage for the determination of the velocity at the next time level.

8. Startup of Poiseuille flow

Although the algorithm described above is valid for two and three-dimensional flows, in this paper, numerical results will be presented only for the startup of Poiseuille flow. Analytically this is a standard intial value problem for the axial velocity W as a function of r, t. For the Oldroyd-B fluid in the case of a suddenly imposed, constant pressure gradient, the analytical solution was obtained by Waters and King [14], and in what follows results labelled as analytic have been computed from their solution. Finite element results were obtained for the fully two-dimensional implementation of the Eulerian–Lagrangian scheme as described above. For the Oldroyd-B fluid (4.11) the retardation/relaxation ratio, a, determines the relative importance of elasticity. The purely elastic (Maxwell fluid) and the purely viscous (Newtonian fluid) cases correspond to a of 0 and 1 respectively. The general performance of the finite element code was found to improve as $a \to 1$, and to degrade in the elastic limit $a \to 0$. This degradation also depends on the Deborah number (De) computed from $4\lambda(1-a)V/R$ where V is the mean velocity at the steady state and R the tube radius. This definition corresponds to the ratio of half the wall normal stress to wall shear stress at the steady state. The level of inertia is measured by Reynolds number (Re) computed from $\rho VR/\eta$. The implicitness coefficient in (3.9) was determined to be -1.5 by minimizing the error in the Newtonian problem. To avoid varying too many parameters, values have been chosen which demonstrate the capabilities of the numerical scheme. Most of the results have been computed at the standard values of $De = 4$, $Re = 1/2$. In the elastic limit the solution for these values exhibits the characteristic oscillatory response to the point of flow reversal.

For the standard values of De and Re and $a = 0.1$ Figs. 2, 3 and 4 show at various times shortly after startup the profiles of axial velocity, elastic shear stress and elastic normal stress components of $\boldsymbol{T}_M$ defined in (4.11). The spatial mesh used in all of these calculations consists of a 4 by 4 arrangement of quadrilaterals on a tube of unit radius and length 3, and contains about 290 V, p unknowns. Except for the results in Fig. 5 all calculations are based on the $O(\Delta t^3)$ approximation for the elastic stress,

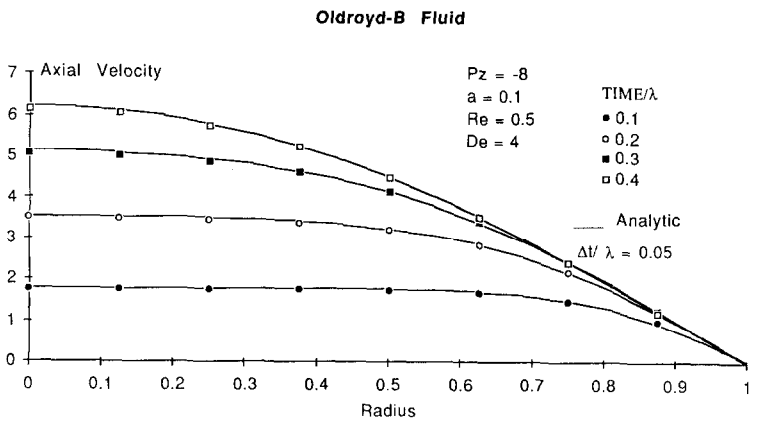

Fig. 2. Axial velocity (W) distribution during startup of an Oldroyd-B Fluid, $a = 0.1$; pressure gradient imposed suddenly at $t = 0$.

equation (4.23). For the stresses double values at the common nodes are plotted without averaging. It can be seen that on the scale of these plots the discontinuities are barely perceptible. Note that shear stress has been normalized with $\eta V/R$ and the normal stress with the steady state shear stress $4\eta V/R$. Centerline values of the velocity and wall values of the stresses are plotted as functions of time of Fig. 5 for the stress approximations (4.10) and (4.23). Generally, agreement with the analytical solution is better for the $O(\Delta t^3)$ approximation. A more revealing measure of perfor-

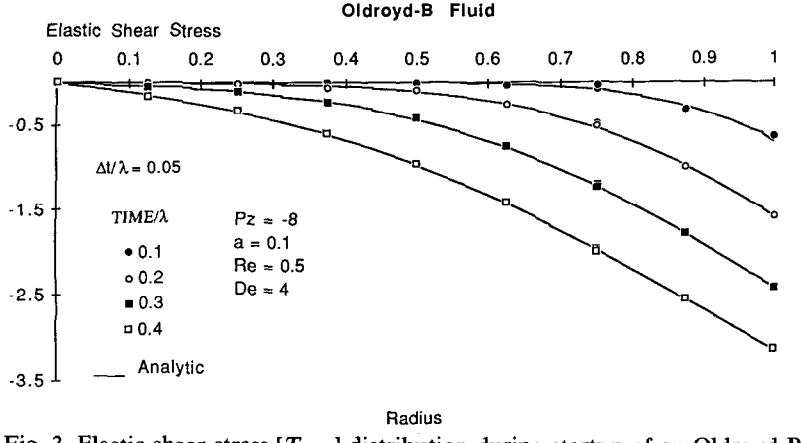

Fig. 3. Elastic shear stress [T_{Mrz}] distribution during startup of an Oldroyd-B Fluid, $a = 0.1$; pressure gradient imposed suddenly at time = 0.

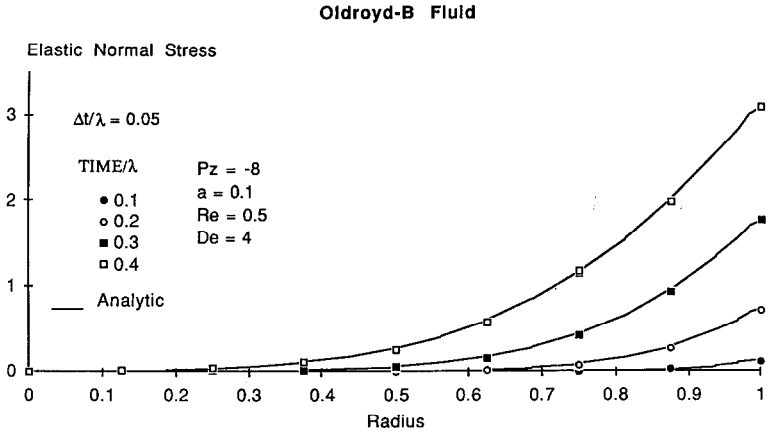

Fig. 4. Elastic normal stress$[T_{M2zz}/T_{Mrz}(1, \infty)]$ distribution during startup of an Oldroyd-B Fluid, $a = 0.1$; pressure gradient imposed suddenly at time = 0.

mance is plotted in Fig. 6 where a composite error is plotted against time. This error is composed from

$$|\delta U| + |\delta p| + |\delta(T_{rr} - T_{\theta\theta})|, \tag{8.1}$$

where the δ differences are taken relative to the analytical solution. The nodal values for the whole domain, at every time level, are surveyed for their maximum from which Fig. 6 has been constructed. The dependence of the

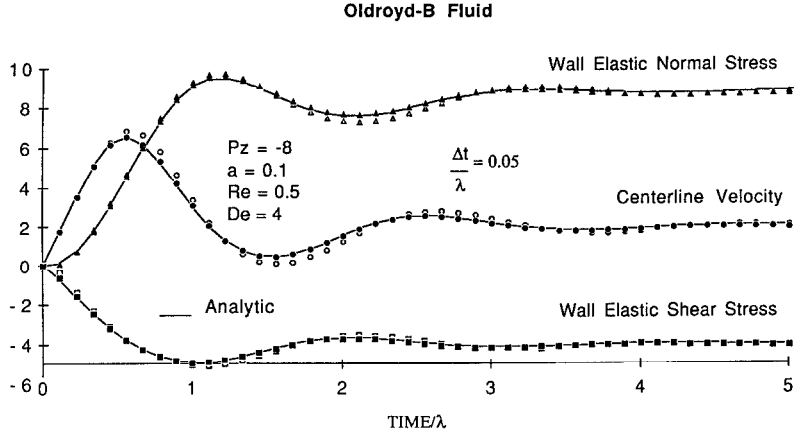

Fig. 5. Centerline velocity $[W(0, t)]$, wall elastic shear stress $[T_{Mrz}(1, t)]$ and wall elastic normal stress $[T_{M2zz}(1, t)/T_{Mrz}(1, \infty)]$ vs. time during startup of an Oldroyd-B fluid, $a = 0.1$; pressure gradient imposed suddenly at time = 0. Solid markers: $O(\Delta t^3)$ stress approximation (eqn. (4.23)). Hollow markers: $O(\Delta t^2)$ stress approximation (eqn. (4.10)).

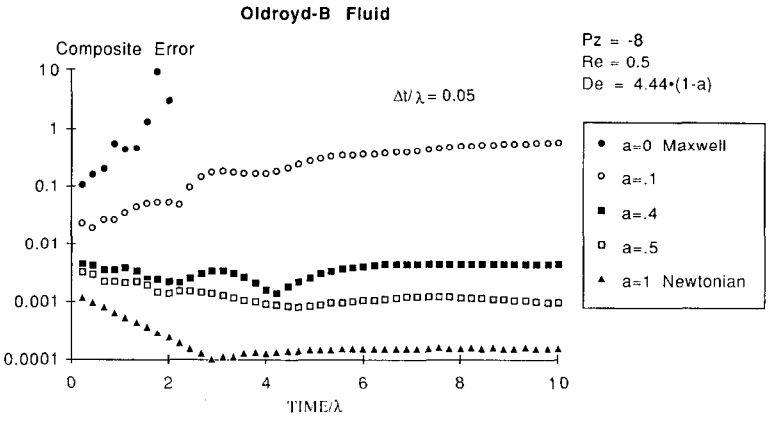

Fig. 6. Composite error (eqn. (8.1)) during startup of Oldroyd-B fluids for various values of a; pressure gradient imposed suddenly at time = 0.

error level on the retardation/relaxation ratio clearly demonstrates that the major source of error originates in the elastic stress as might be expected. At $a = 0.1$ convergence is marginal at $De = 4$, and improves at lower De or larger a values.

The capability of handling multimode fluids is demonstrated with the low density polyethylene spectrum used by Luo and Tanner [11]. In order to make meaningful comparisons with the startup problem for the single mode case the relaxation spectrum, given in Table 1, is scaled with the mean relaxation time and the total viscosity. The latter are then chosen so that in the steady state the stress system is identical to that of the single mode fluid, i.e. De and Re are based on the mean relaxation time and the total viscosity. Fig. 7 shows the centerline velocity for the jump start and the same flow conditions used to produce Fig. 5. It is seen that the oscillatory

TABLE 1

Spectrum for multimode fluid from Ref. 11. $\lambda = 58.7$ s and $\eta = 5{,}110$ Pa s

i	λ_i/λ	η_i/η
1	1.70E+1	1.96E−2
2	1.70E+0	3.53E−1
3	1.70E−1	3.70E−1
4	1.70E−2	1.92E−1
5	1.70E−3	5.23E−2
6	1.70E−4	1.15E−2
7	1.70E−5	1.86E−3
8	1.70E−6	2.53E−4

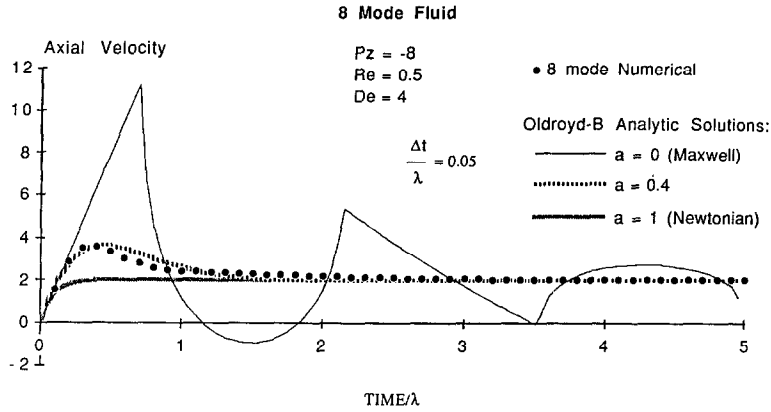

Fig. 7. Centerline velocity ($W(0, t)$) during startup of an 8-mode Fluid; pressure gradient imposed suddenly at time = 0. Superimposed are the Maxwell, Newtonian, and Oldroyd-B ($a = 0.4$) analytical solutions.

response which characterizes the single mode fluid is greatly attenuated by the spectral dispersion of the elastic response of the material.

The startup problem contains some inherent difficulties for numerical analysis, and these effects are amplified in the important limit of vanishing inertia at finite Deborah number. In the purely elastic case the startup problem is characterized by the propagation of shear waves which initiate at the walls, propagate inwards, and reflect from the centerline. The amplitude (vorticity jump) of these waves attenuates as $\exp(-t/2\sigma)$. For the Maxwell fluid σ and λ are identical so that wave effects will dominate the solution for most of the transient. For the multimode fluid $\sigma \ll \lambda$; hence the waves will have only a fleeting existence. In Fig. 8 velocity profiles are shown for the Maxwell fluid ($a = 0$) for the conditions of Fig. 2. It is obvious that the numerical scheme does not simulate the flow in the viscinity of the discontinuities, and this is also evident from the error growth with time shown in Fig. 6. The wave speed is given by $\sqrt{G_0/\rho}$, and hence is infinite in the limit $\rho \to 0$. This means that in the regime of small inertia waves reflect with essentially infinite frequency. Because of this the analytical solution [14] is difficult to plot for the Maxwell fluid; for the Oldroyd-B fluid at small *Re* and *De* of 4 the numerical solution is compared to the analytical solution in Fig. 9. The very rapid rise of the centerline velocity from zero to a maximum is omitted for clarity. The numerical solution effectively jumps over this phenomenon with little loss of accuracy. For the multimode fluid the results of a similar numerical calculation are displayed in Fig. 10. The time scale is logarithmic to permit the response at very small times to be examined closely. The smallest time step is two orders of magnitude greater than the

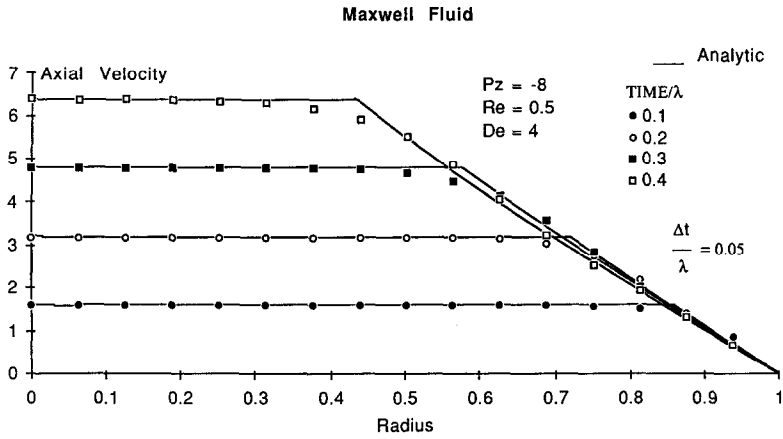

Fig. 8. Axial velocity (W) distribution during startup of a Maxwell Fluid; pressure gradient imposed suddenly at time = 0.

smallest relaxation time. During the initial phase the numerical solution is evidently dependent on the magnitude of Δt. It can be seen that after an initial oscillatory response for the first few time steps the solution approaches a common, smooth curve which is independent of the time steps. These results suggest that at times comparable to the smallest relaxation time the centerline velocity will rise almost instantaneously to a very high peak. The analytical curve for the Oldroyd-B fluid for the same *Re* and *De* is plotted for comparison. There is no value of the retardation/relaxation ratio which brings these curves into agreement.

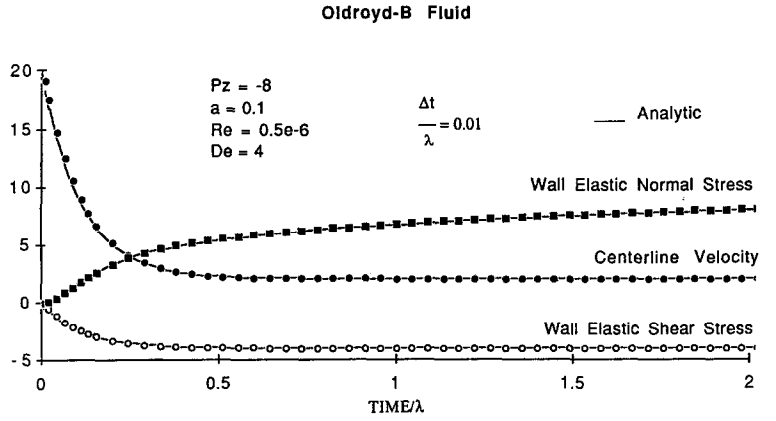

Fig. 9. Centerline velocity [$W(0, t)$], wall elastic shear stress [$T_{Mrz}(1, t)$] and wall elastic normal stress [$T_{M2zz}(1, t)/T_{Mrz}(1, \infty)$] vs. time during startup of an Oldroyd-B fluid at low *Re*, $a = 0.1$; pressure gradient imposed suddenly at time = 0.

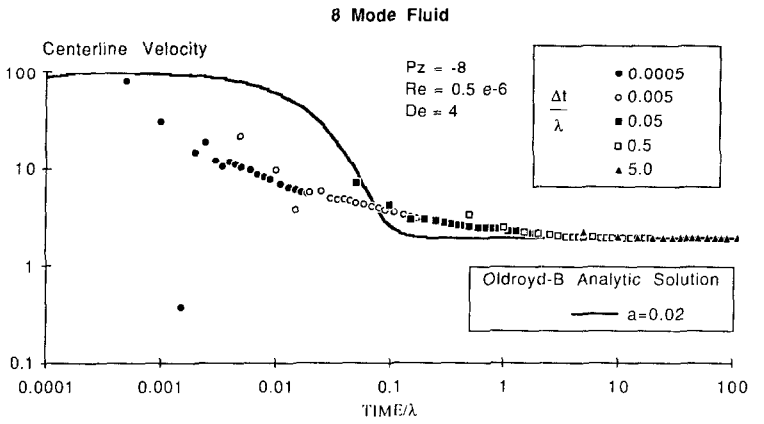

Fig. 10. Centerline velocity ($W(0, t)$) during startup of an 8 Mode Fluid at low Re; pressure gradient imposed suddenly at time = 0. Superimposed is the Oldroyd-B ($a = 0.02$) analytical solution.

The same initial condition on the pressure gradient has been used in all of the cases presented above. For viscoelastic fluids in the low Re limit this initial condition gives rise to a singularity whose manifestation is extreme for the Maxwell fluid. Alternatively, imposing the mean velocity gives rise to a pressure singularity [15]. Since any numerical scheme will degrade in the vicinity of a singularity it is of interest to find out if a milder initial condition can eliminate some of the extreme behaviour. The initial value problem of Waters and King [14] has been solved for the case when the

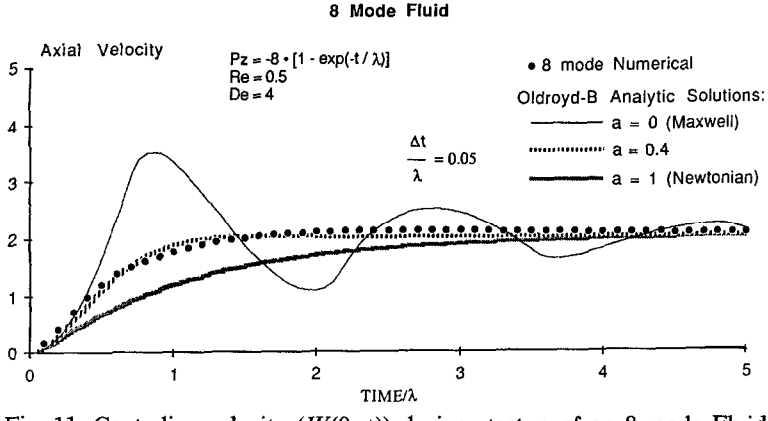

Fig. 11. Centerline velocity ($W(0, t)$) during startup of an 8-mode Fluid; pressure gradient imposed exponentially. Superimposed are the analytical solutions for the Maxwell fluid, Oldroyd-B fluid [$a = 0.4$], and Newtonain fluid with $\lambda = 2R^2\rho/\eta$.

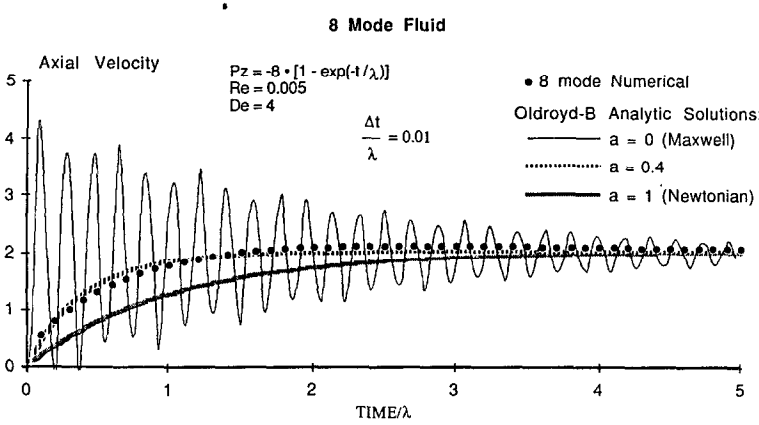

Fig. 12. Centerline velocity [$W(0, t)$] during startup of an 8-mode fluid at low Re; pressure gradient imposed exponentially. Superimposed are the analytical solutions for the Maxwell fluid, Oldroyd-B fluid [$a = 0.4$], and Newtonian fluid with $\lambda = 2R^2\rho/\eta$.

pressure gradient is $P_z[1 - \exp(-t/\lambda)]$, $t > 0$. This loading rate ensures against the sudden imposition of pressure. The curves in Fig. 11 display the time evolution of the centerline velocity for the multimode fluid; in the pressure loading term λ is the mean relaxation time. The analytical response for the Maxwell fluid, the Oldroyd-B fluid and the Newtonian fluid are also plotted for comparison. Note that the viscous time scale is used to accommodate the Newtonian case. For the Maxwell fluid profiles of velocity similar to Fig. 8 appear to be smooth which means that the vorticity jump at the wave fronts has been reduced nearly to the vanishing point. This is consistent with the absence of cusps in the time evolution of the centerline velocity displayed in Fig. 11. For the Newtonian fluid the pressure loading rate parameter λ is arbitrary, and has been chosen to be the same number as in the viscoelastic case. Figures 11, and 12 show the response of single and multimode fluids to be distinct. In the absence of a singular startup condition the Maxwell fluid response is oscillatory with frequency increasing as $Re \to 0$. The only essential difference between the gradually and the suddenly imposed pressure conditions is the amplitude of the oscillations which initially approaches infinity for the jump start. For the multimode case the response to a regular loading rate is very nearly viscous. Viscoelastic overshoot such as is shown in Fig. 7 is to be expected only from a singular loading rate.

9. Conclusion

An Eulerian–Lagrangian scheme for the calculation of time dependent flows has been derived in detail for the case of the Maxwell fluid, the

Oldroyd-B fluid and for the rubberlike fluid. The method has been demonstrated numerically for the startup of Poiseuille flow. It has been shown how Eulerian statements can be generated from Lagrangian time expansions which allow the solution of the constitutive equation to be separated from the solution of the conservation laws. In this work expansions of $O(\Delta t^3)$ have been obtained without the appearance of second gradients as suggested in earlier work [1]. The implications for numerical simulation are that since V, p variables are obtained separately from stress variables the vector of unknowns in the spatial problem is the same for single mode or multimode fluids. In this work the stresses are updated explicitly, element-by-element, after the spatial equations have produced the velocity field in each time step.

The present formulation is not satisfactory in the strongly elastic case. Two causes have been identified. The first is that for the Maxwell fluid the transient is dominated by shear waves which are not modelled with the finite elements used here. The second has been identified as the method for fitting nodal stresses from Gauss point values in the stress updating step. It can be shown that the least squares fit is biased, and gives rise to axial oscillations of stress in the one-dimensional problem studied in this work. Numerical experiments were carried out in which the amplitude of the oscillations was controlled by axial stretching of the elements by factors of 10, 100, ... With this artifice it was possible to maintain convergence for the Maxwell model at De values as high as 40. Improvements in the representation and the updating of the stresses are under investigation, and will be reported in future work.

Although the results presented here are limited to a one-dimensional flow problem some insights have been gained about the differences between the response of single and multimode fluids. It follows from Figs. 11 and 12 that the Maxwell fluid has a singular limit as $Re \to 0$ at constant De. The tendency towards oscillations at finite frequency is independent of the initial conditions. Similar behaviour is found for the jump start for which the initial amplitude is unbounded as $Re \to 0$. In contrast, the multimode fluid response to a gradually applied load is nearly viscous. A singular loading rate, such as the jump start, gives rise to an overshoot type of response. Provided the startup is regular the response of the multimode fluid can be simulated with a single mode Oldroyd fluid with a suitable choice of retardation parameter. However, this will not work in the important low Re limit if the loading rate is singular. In general, the single mode models with small retardation times appear to greatly exaggerate elastic effects, and do so especially in the nearly inertialess regime.

Acknowledgement

Support for this work by the National Science MSM 82170 is gratefully acknowledged.

References

1 B. Caswell, An Eulerian–Lagrangian formulation for the numerical simulation of viscoelastic flow, in: B. Mena, A. García-Rejón and C. Rangel-Nafaile (Eds.), Advances in Rheology, Vol. 1, Elsevier, Amsterdam, 1984, pp. 259–267.

2 B. Caswell, Lagrangian concepts for the numerical analysis of viscoelastic flow, in: C. Dafermos, J.L. Ericksen and D. Kinderlehrer (Eds.), Amorphous Polymers and Non-Newtonian Fluids, IMA Volumes in Mathematics and Its Applications, Vol. 6, Springer-Verlag, Berlin, 1987, pp. 21–32.

3 O. Hassager and C. Bisgard, A Lagrangian finite element method for the simulation of the flow of non-Newtonian fluids, J. Non-Newtonian Fluid Mech., 12 (1983) 283–302.

4 S. Neuman, Adaptive Eulerian–Lagrangian finite element method for advection–dispersion, Int. J. Numer. Meth. Eng., 20 (1984) 321–337.

5 J.P. Huffenus and D. Khaletzky, The Lagrangian approach of advective term treatment and its application to the solution of the Navier–Stokes equations, Int. J. Numer. Meth. Fluids, 1 (1981) 365–387.

6 M. Viriyayuthakorn and B. Caswell, Finite element simulation of viscoelastic flow, J. Non-Newtonian Fluid Mech., 6 (1980) 245–256.

7 I. Fried, Numerical Solution of Differential Equations, Academic Press, New York, NY, 1979.

8 D. Malkus and B. Bernstein, Flow of a Curtiss–Bird Fluid over a transverse slot using the finite element drift function method, J. Non-Newtonian Fluid Mech., 16 (1984) 77–116.

9 M. Crochet, J.S. Dupont and J.M. Marchal, The numerical simulation of the flow of viscoelastic fluids of the differential and the integral types: A comparison, in: B. Mena, A. Garcia-Rejón and C. Rangel-Nafiale (Eds.), Advances in Rheology, Vol. 1, Elsevier, Amsterdam, 1984, pp. 129–147.

10 A.C. Papanstasiou, L.E. Scriven and C.W. Macosko, A finite element method for liquid with memory, J. Non-Newtonian Fluid Mech., 22 (1987) 271–288.

11 X.L. Luo and R.I. Tanner, A streamline element scheme for solving viscoelastic flow problems, Part II: Integral constitutive equations, J. Non-Newtonian Fluid Mech., 22 (1986) 61–89.

12 A.S. Lodge, A network theory of flow birefringence and stress in concentrated polymer solutions, Trans. Faraday Soc., 52 (1956) 120–130.

13 R.E. Nickel, R.I. Tanner and B. Caswell, The solution of the viscous incompressible jet and free surface flows using finite element methods, J. Fluid Mech., 65 (1974) 189–206.

14 N.D. Waters and M.J. King, The unsteady flow of an elastico-viscous liquid in a straight pipe of circular cross-section, J. Phys. D, Appl. Phys., 4 (1971) 204–211.

15 M.E. Ryan and A. Dutta, Analysis of the constant rate startup flow of a viscoelastic fluid in annular, cylindrical, and planar conducts, J. Rheol., 25 (2) (1981) 193–212.

16 C. Truesdell and R. Toupin, Principles of classical mechanics and field theory, in: Handbuch der Physik III/1, Springer-Verlag, Berlin, 1960.